4

Modeling and Optimization of Three-Dimensional Interdigitated Lateral p-i-n Photodiodes Based on $In_{0.53}Ga_{0.47}As$ Absorbers for Optical Communications

P Susthitha Menon, Abang Annuar Ehsan and Sahbudin Shaari
Universiti Kebangsaan Malaysia, Bangi, Selangor
Malaysia

1. Introduction

Access networks such as Fiber-to-the-Home based on passive optical networks (FTTH-PON) are experiencing a paradigm shift where these 'last-mile' networks are experiencing the need to provide converged services to the end-user at home. Triple-play services such as data and voice operating at the optical wavelength, λ=1310 nm as well as video (λ=1550 nm) at a minimal speed of 2.5 Gbps are demanded to achieve an all-optical-network revolution (Kim, 2003; Lee & Choi 2007). It is estimated that in 2011, there will be 10.3 million FTTH households in the USA alone (Lee & Choi 2007). Thus, there arises a need to produce optical components which can be fabricated easily and in a cost-effective manner to cater for this ever-increasing demand.

The development of interdigitated lateral p-i-n photodiodes (ILPP) based on $In_{0.53}Ga_{0.47}As$ (InGaAs) absorption layer can be achieved using cheap and easy CMOS fabrication techniques such as diffusion and ion implantation. This can cater for the ever increasing demand of fiber-to-the home passive optical access networks (FTTH-PON) operating at a minimal speed of 2.5 Gb/s. The InGaAs ILPP which converts optical signals to electrical signals in the optical receiver has advantages compared to other photodiode structures because it has a high-resistance intrinsic region thus reducing Johnson noise, has low dark currents, permits a large detection area along with a low device capacitance, and can be monolithically integrated with planar waveguides or other devices. This chapter summarizes our key results on the modeling, characterization and optimization of ILPP based on $In_{0.53}Ga_{0.47}As$ absorbers for optical communications. A three dimensional model of ILPP InGaAs operating at the optical wavelength, λ of 1.55 μm was developed using an industrial-based numerical software with a proposed fabrication methodology using spin-on chemicals. New parameters for three different carrier transport models were developed and the proposed design was characterised for its dark and photo I-V, responsivity, -3dB frequency and signal-to-noise ratio (SNR) values. Statistical optimization of the InGaAs ILPP model was executed using fractional factorial design methodology. Seven model design factors were investigated and a new general linear model equation that relates the responsivity to significant factor terms was also developed (Menon, 2008; Menon et al.,2008a; Menon et al., 2008b; Menon et al. 2009)

2. Application, fabrication and simulation of lateral P-I-N photodiodes

2.1 The application of ILPP

Else than optical communication systems, InGaAs-based photodiodes are also used in optical measurement systems such as for high precision length measurement, light patterns, spectrum analyzer, speed measurement in luminuous flow as well as in imaging applications. Other application include high speed sampling, optoelectronic integrated circuits (OEIC), high speed device interconnects, optoelectronic mixers and also for microwave single sideband modulation.

Photodiode design structures can be categorised based on the illumination direction, detection mechanism and the structure itself. The illumination direction of a photodiode can be classified into two; the vertical illuminated photodiode (VPD) and the edge illuminated photodiode which is known as the waveguide photodiode (WGPD). VPDs are the preferred photodiodes for OEICs due to its planar structure but the layers in VPDs are grown epitaxially using complex fabrication methods. Meanwhile WGPDs overcome the limitation of the bandwidth-efficiency product in VPDs because the electrical transit of carriers are perpendicular to the optical propagation direction. Photodiodes can also be classified based on the detection mechanism such as the avalanche photodiode (APD) or the p-n junction photodiode where the former has sensitivity limits of 5-10 db higher than the latter due to the multiplication region at the absorption layer hence producing high gains.

The structure of photodiodes can be divided to p-i-n types or metal-semiconductor-metal (MSM) types (inclusive of Schottky photodiodes). Vertical p-i-n photodiodes consist of one p+ doped layer at the topmost region followed by the absorption (intrinsic) layer in the middle and finally the n+ dope region at the bottom. MSM photodiodes have metal fingers deposited on the semiconductor and photons are detected via collection of electron-hole pairs that experience drift due to the presence of the electric field between the metal fingers (Zhao, 2006).

The internal gain mechanism in APDs makes it suitable to be used in long distance fiber optic transmission systems. However, the impact ionization produces additional noise in APDs and reduces the signal-to-noise ratio (SNR). Else than that, APDs are costly, hence they are normally not utilized in medium and short-haul optical communication systems (Huang, 2003). MSM photodiodes have lower capacitances compared to VPDs for the same amount of device active area. It is also a planar structure and can be integrated wasily with MESFET-based pre-amplifiers. However, the fabrication of MSM photodiodes is not compatible with CMOS processes where ohmic junctions are preferred compared to metal junctions (Menon, 2005). MSM photodiodes also have a larger dark current compared to p-i-n photodiodes (Koester et al., 2006).

In this chapter, we will discuss about the formation a p-i-n photodiode structure which is a combination of WGPD and MSM photodiodes and is known as the interdigitated lateral p-i-n photodiodes (ILPP). It can be given surface or edge illumination such as in the WGPD but the arrangement of the p, i and n region are in a planar form. Interdigitated electrodes such as those used in MSM photodiodes reduces the device capacitance and increases the area of optical absorption. The planar structure eases monolithic integration compared to a vertical structure (Koester et al., 2006). Moreover, the ILPP can be fabricated using standard CMOS processes such as diffusion or ion implantation. Fig. 1 shows the differences between different photodiode structures.

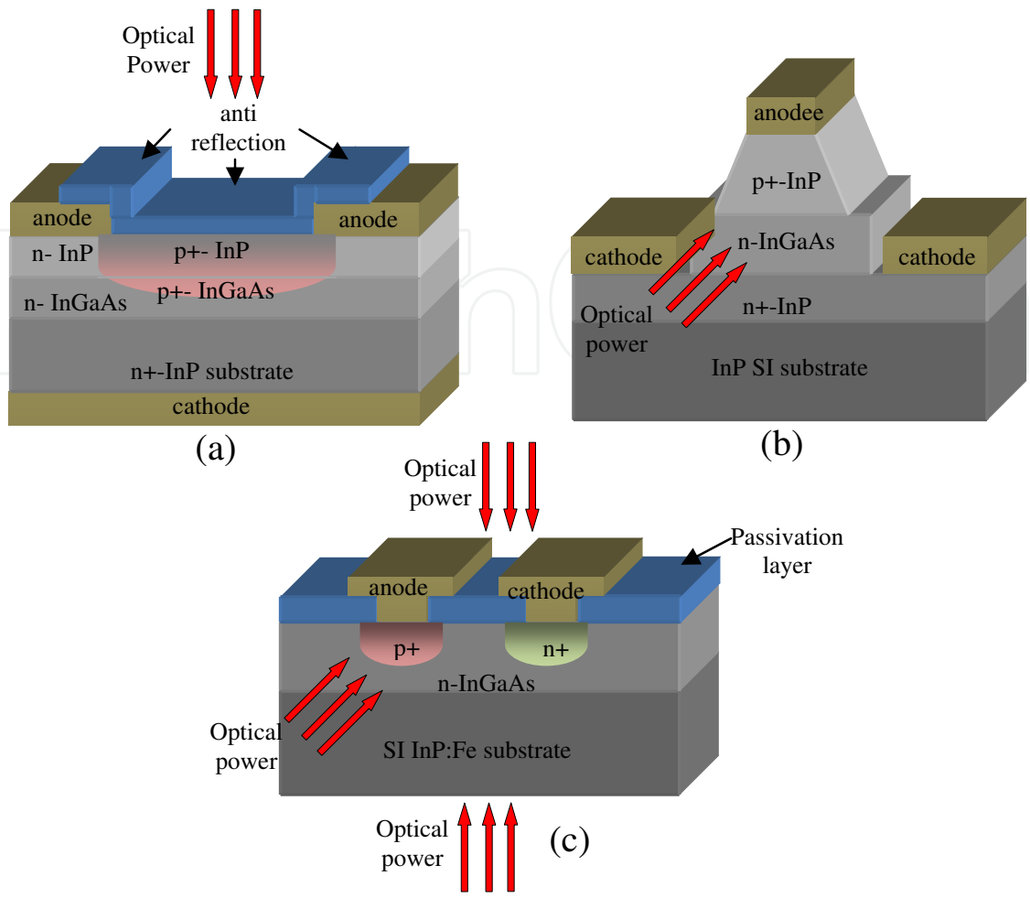

Fig. 1. Various p-i-n photodiode design structures based on InP substrate for (a) VPD, (b) WGPD and (c) ILPP

2.2 III-V Material: In(0.53)Ga(0.47)As

At optical wavelengths of 1.55 µm, III-V semiconductor materials are normally used because the energy gap can be modified according to the intended wavelength by changing the relative composition of the material which is lattice-matched to the substrate. Three basic alloy systems which are useful for telecommunication applications are AlGaSb, InGaAs and HgCdTe. Although all three ternary materials can be used for the development of an ILPP, InGaAs remains as the preferred choice due to the available technology for laser, LED and diodes fabrication developed from this material as well (Tsang, 1985). Indium gallium arsenide (InGaAs) is a III-V material that consist of indium, gallium and arsenide components. It is used in high power and high frequency optoelectronics applications due to the high electron and hole saturation velocity (~6 x 10^6cm/s and ~4.6 x 10^6 cm/s) as well as the high absorption coefficient (0.65 μm^{-1} at λ=1.55 µm). The electron mobility in InGaAs is 1.6 times higher than GaAs and is 9 times higher compared to Si (Sze, 2002). The energy gap of InGaAs which is 0.75 eV at optical wavelength of 1550 nm makes it a suitable material to be used as a detector in fiber optic communication systems both at 1300 and 1550 nm wavelengths.

The indium content in InGaAs determines the two dimensional charge carrier density. The optical and mechanical properties of InGaAs can be modified by changing the ratios of

indium and gallium to form $In_xGa_{1-x}As$. InGaAs-based devices is normally developed on indium phosphide (InP) substrates which has a energy gap of 1.35 eV. To match the lattice constant of InP dan to avoid mechanical strain, the commonly chosen composition is $In_{0.53}Ga_{0.47}As$ where the cut-off wavelength is at 1.68 µm. By increasing the ratio of In compared to As, the cut-off wavelength can be increased upto 2.6 µm. The lattice constant and cut-off wavelength for alloys that produce InGaAs is shown in Fig. 2.

A high electron mobility transistor (HEMT) utilizing InGaAs channels is one of the fastest transistors which can achieve speeds upto 600 GHz. InGaAs is a popular material in infra-red photodiodes and is replacing Ge as a photodiode material mainly because of the low dark current whereas in APDs, the multiplication noise in the active multiplication region based on InGaAs is much lower compared to Ge. Therefore, the technology and applications based on InGaAs material is wide and its usage as the absorbing layer in an ILPP is most appropriate for the current trends (Menon, 2008).

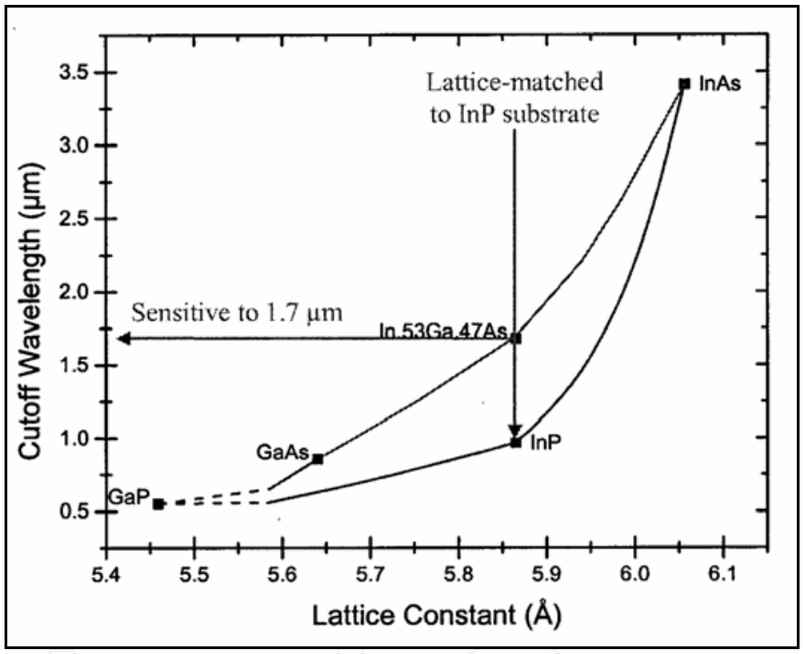

Fig. 2. Lattice constant and cut-off wavelength for alloys that produce InGaAs (Source: Goodrich, 2006)

2.3 Review of fabricated InGaAs/InP-based ILPP

The ILPP structure has been developed on many different substrates utilizing different material as the absorbing layer depending on the respective wavelengths. These include silicon (Schow et al., 1999), silicon-on-SOI (silicon-on-insulator) (Li et al., 2000), Ge-on-SOI (Koester et al., 2006) and GaAs (Giziewicz et al. 2004).

ILPP on InGaAs/InP substrates were developed by Lee et al (1989) which was integrated with an InP-based JFET amplifier. The p+ well was formed using ion implantation using Mg+ at 25 keV and dosage of 1 x 10^{14} cm^{-2}. The thickness of the InGaAs absorption layer was 2 μm. The width and length of the fingers were 2 μm and 47 μm respectively. Distance between the p+ and n+ fingers was 3 μm and the total active area space was 50 μm x 50 μm. Optical sensitivity of -29 dBm was achieved at a bit rate of 560 Mbit/s. Leakage current and

capacitance was measured to be 1.5 μA and 130 fF. Responsivity value achieved was 0.56-0.6 A/W at optical wavelength of 1.3 μm.

Diadiuk & Groves (1985) produced a lateral p-i-n photodiode on a semi-insulating (SI) InGaAs substrate developed using the Liquid Phase Epitaxy (LPE) technique. Metal contacts consisting of AuZn and NiGeAu were deposited on the InGaAs layer with thicknesses of 2-4 μm. Dopant from the metal electrodes will diffuse into the semiconductor during the alloying process and subsequently p+ and n+ junctions are formed. Interdigitated electrode structure without an anti-reflecting layer has finger lengths of 300 μm and width of 100 μm where distance between fingers is 3 – 20 μm. The capacitance was ~ 18 pF (electrode distance 3 μm) whereas the quantum efficiency is ~40% at λ=1.24 μm. Breakdown voltage was at 50 V and the leakage current was < 1 nA at bias voltage of 0.9 V. The response time in the InGaAs substrate was 50 ps (FWHM) where f_{-3dB}=0.4/50 ps = 8 GHz for devices with finger distances of 3 μm.

A lateral p-i-n photodiode utilizing InGaAs as the absorption layer on InP substrate was developed by Yasuoka et al. (1991). Monolithic integration was achieved using a coherent receiver with waveguide coupling with a pair of interdigitated lateral p-i-n photodiodes. The -3dB frequency was at 2 GHz and quantum efficiency was 85 % at λ=1540 nm at a bias voltage of 5 V. The p+ well was formed using Zn diffusion via a SiN_x layer to form the p+ InP junction whereas the n-InP cap layer acted as the n+ region. Dark current value was < 10 nA until bias voltages of 12 V and the capacitance was 0.3 pF at V = 5V.

A planar p-i-n photodetector based on InGaAs substrate was fabricated using self-aligned contact technique (Tiwari et al., 1992). The p-type and n-type contacts were formed using W (Zn) and $MoGe_2$ metalurgy. Bandwidths exceeding 7.5 GHz and responsivity of 0.53 A/W was achieved by this device with bias voltage of 5 V and optical wavelength of 1.3 μm. Jeong et al. (2005) developed an InGaAs-based ILPP comprising of p+ and i regions to be integrated with a two terminal heterojunction phototransistor (2T-HPT). The photodiode which was fabricated using epitaxial methods with InGaAs absorption layer thickness of 800 nm achieved bandwidths of 100 MHz due to surface leakage current phenomena at the exposed InGaAs surface layer. Responsivity was at 0.21 A/W for a device size of 20 μm x 20 μm. Lateral p-i-n photodiodes based on InGaAs/InP usually achieve quantum efficiencies of 50-90%, responsivity of ~ 1 A/W and bandwidth upto ~60 GHz (Saleh et al., 1991).

2.4 Spin-on chemical fabrication method of InGaAs/InP-based ILPP

Normally, p-type dopants are incorporated into InGaAs or InP layers using a closed-tube system where the substrate and the dopant powder source are placed in an ampoule (Ho et al., 2000; Feng & Lu, 2004). Air in the capsule is released until low pressure is achieved and the capsule is sealed. Then the capsule is placed in a furnace and heat evaporates the dopant source and produces dopant vapour that will diffuse into the substrate. The diffusion is uniform due to the non-existence of air in the capsule. However, the costly capsule as well as the vacuum pump causes this process not to be preferred.

Solid phase diffusion (SPD) is a doping technique without rays and examples of SPD include dopant diffusion from doped epitaxial layers, doped oxide layers and spin-on dopants (SOD). The SOD technique is a common SPD technique where a conformal layer is spun-on the surface of the substrate. This dopant source consists of oxide powder mixed with a solvent. Substrates which are covered with dopants are heated to evaporate the solvent and leave a doped oxide layer which is compatible with the substrate surface. Next,

the substrate is placed in a deposition tube where annealing treatment will release the dopant from the oxide and aim it into the substrate. SODs have the potential to produce high uniformity and productivity. Common problems that would arise are such as dopant spreading in the oxide layer, thickness variation especially during the early stages and cost related to additional processes such as etching and annealing (Zant, 2000).
The SOD technique have been used to produce the p+ and n+ wells in silicon substrates (Gangopadhyay et al. 2003; Oh et al. 2004), n+ wells in germanium layers (Posthuma et al. 2007) as well as the p+ and n+ wells in GaAs substrates (Filmtronics, 2006a; Filmtronics, 2006b). In addition, the SOD diffusion technique was used previously in the development of a silicon-based lateral p-i-n photodiode in our laboratory (Ehsan & Shaari, 2001; Menon, 2005).
In InGaAs/InP-based substrates, the p+ wells were produced using the SOD technique by several researchers (Lange et al. 2000; Kamanin et al. 1996 & Lauterbach 1995). The quality of the p+ junctions is at par with those produced using the closed ampoule technique (Lange et al. 2000). However, based on the literature survey, the SOD technique has never been used to produce the n+ junction in InGaAs/InP substrates. Normally, n-InGaAs is produced using silicon as a dopant (Si_2H_6 in H_2) which is diffused into the InGaAs layer during the epitaxial layer growth process (Murray et al. 2003). Another option is to dope the InP epitaxial layer with sulphur or Si (Dildey et al, 1989). Therefore, in this project, the SOD technique is used for the first to time to produce both the p- and n-type wells in the absorbing InGaAs layer in an ILPP device (Menon et al. 2010).

2.5 Review of simulated InGaAs/InP-based ILPP

The simulation of optoelectronic devices such as lateral p-i-n photodiodes require accurate modeling based on semiconductor physics principles. Generally, semiconductor device equations can be solved using two methods; a fully numerical approach or an analytical approach. For models that are used in circuit simulation, the latter is more suitable because the computation time can be reduced whereas the former approach is more appropriate in simulation of optoelectronics devices simulation. The numerical approach can be divided to Monte-Carlo (MC) based simulation or solving the approximation of the drift-diffusion (DD) equation where a solution for the Boltzmann transport equation can be obtained (Konno et al., 2004). Nowadays, there are many device simulators which are developed using the DD equation solution.
In the modeling the ILPP device, various methods have been used before this. Konno et al. (2004) has used the analytical model in the Fourier space as well as numerical method to characterize a silicon-based p-i-n photodiode. The analytic analysis for the frequency response for an InGaAs-based p-i-n photodiode was undertaken by Sabella & Merli (1993). A numerical analysis on the non-linear response of InGaAs-based photodiode at high illumination conditions was also performed previously (Dentan & Cremoux, 1990). A numerical model for an InGaAs-based p-i-n photodiode which utilizes the pulse response equation was developed by Cvetkovic et al. (2000). Software such as SPICE and MATLAB has also been utilized previously to perform numerical simulation on p-i-n photodiodes (Parker, 1988; Loo, 2007).
Semiconductor device software such as MEDICI was used by Li et al. (2000) to simulate an ILPP device based on silicon. Numerical software such as ATLAS from Silvaco Inc. can be used to develop two and three dimensional models of semiconductor devices. Prior to this, this software was used to develop semiconductor devices such as an avalanche photodiode

(Lee et al., 2004), a uni-travelling photodiode (UTC-PD) (Srivastava & Roenker, 2003), a vertical photodiode (Jacob et al. 2005) and a silicon-based lateral p-i-n photodiode (Menon, 2005).

In this work, Silvaco Atlas was used, for the first time, to develop a three dimensional model of an interdigitated lateral p-i-n photodiode based on InGaAs. The 3D analysis takes into consideration the Poisson equation, electron and hole continuity equation, the concentration-dependent minority carrier lifetime model, the concentration-dependent carrier mobility model, Shockley-Read-Hall (SRH) recombination model, Auger recombination model, optical recombination model and the Fermi-Dirac statistics model. Curve fitting methodology using MATLAB was used to obtain parameters of empirical equations used to derive the minority carrier lifetime and the carrier mobility. The developed model was characterized for its responsivity, -3dB frequency, I-V, C-V and the signal-to-noise ratio (SNR) (Menon, 2008; Menon et al.,2008a; Menon et al., 2008b; Menon et al. 2009, Menon et al. 2010).

2.6 Statistical modeling

The design of experiment (DOE) was created by the British scientist, Sir R. A. Fisher in the 1920-es. The fractional factorial design (FFD) is one the methodologies in DOE design based on statistical consideration that brings about meaningful information about the effects of design parameters on the device characteristics. Other famous statistical methods include the Monte-Carlo and the worst-case statistical method. The advantages of FFD are it can save experimental time because the number of simulation experiment which needs to be executed can be reduced with the assumption that all variables have no interactions.

The FFD technique has been used before in both device simulated modeling as well as in device fabrication. Sipahi & Sanders (2002) used the FFD technique to investigate parameters that affect the simulated model of a low noise amplifier whereas Yuan et al. (2005) applied the FFD technique with a resolution IV in the simulation of their silicon-based chip packaging model. Jacob et al. (2006) used the full factorial design to optimise the characterisation of design parameters in the simulation of a photodiode for imaging applications.

Therefore, the simulated ILPP model was optimised prior to the fabrication process. Seven design factors at two levels each i.e., the thickness of the InGaAs absorption layer, the distance between the finger electrodes, the junction depth, the width of the interdigitated finger electrodes, the bias voltage and the input optical power were investigated. A resolution IV fractional factorial design (Montgomery, 2005) was executed to identify the effects of these factors on the key characteristics of an ILPP which are the responsivity, the -3dB frequency and SNR where a general linear model for all three characteristics was developed respectively using FFD.

3. Theoretical modeling

3.1 Material and model parameters

Semiconductor devices can be modelled in two ways; the first is through the determination of the electrical properties at the device's terminal based on data fitting of empirical results or via the second method; analysis of the carrier transportation processes which occurs in the device. Both these methods were utilized in this research based on the physical model of the device which can determine the terminal characteristics and the carrier transport behaviour within

the device. The physical model of the device was developed based on the description of the substrate material properties and the carrier transport physics. A semiconductor device software, ATLAS from Silvaco International was used simulate the ILPP. It is a numerical simulator which uses differential equations that defines the device physics at different locations within the device. The performance analysis is achieved via self-consistent solution of basic equations that define semiconductor equations such as the Poisson's equation, carrier continuity equations and the current density equations in two or three dimensions. The solution to these equations is based on the device structure, its geometry and the boundary limits which is determined by the electrical contacts and the bias voltage (Silvaco, 2004). The three dimensional analysis takes into account the following physical models; concentration-dependent minority carrier lifetime model, concentration and temperature-dependent mobility model, parallel field mobility, Shockley-Read-Hall (SRH) recombination model, Auger recombination model, optical generation/radiative recombination model and Fermi-Dirac statistics. The material and model parameters were taken from periodical literature (Silvaco, 2004; Srivastava & Roenker, 2003; Adachi, 1992; Datta et al., 1998). Table 1 provides a summary of the material parameters used in this modelling (Menon et al. 2010). The complete list of model and material parameters can be obtained from (Menon, 2008)

Parameter	**Symbol**	**$In_{0.53}Ga_{0.47}As$**
Energy gap	E_g (eV)	0.734
Electron effective mass	m_e^*/m_o	0.033
Hole effective mass	m_h^*/m_o	0.46
Light hole	m_{lh}^*/m_o	0.01
Heavy hole	m_{hh}^*/m_o	0.46
Real index		3.6
Imaginary index		0.08

Table 1. Summary of material parameters used in the modelling (Menon, 2008; Menon et al. 2010)

3.2 Concentration-dependent minority carrier lifetime model

In ATLAS (Silvaco, 2004), the minority electron and hole lifetimes are given by

$$\tau_n = \frac{TAUN\,0}{1 + \frac{N}{NSRHN}} \tag{1}$$

$$\tau_p = \frac{TAUP0}{1 + \frac{N}{NSRHP}} \tag{2}$$

where N is the total impurity concentration and $NSRHN$ and $NSRHP$ are the critical doping concentration above which impurity scattering dominates. Experimental data of electron lifetime (Tashima et al., 1981) in p+-InGaAs was fitted into a simple exponential form as follows (Conklin et al., 1995)

$$\tau_n(n\sec) = 10^{\beta-\gamma\log N_A} \tag{3}$$

where N_A is the p+-InGaAs doping and parameter values of β=12.6, γ=0.73 for N_A > 8x10^{17} /cm^3 were obtained. For smaller base doping than 8x10^{17} /cm^3, a constant lifetime of 0.3 ns was assumed. Similarly for the n+ InGaAs, the hole lifetime is a function of doping and can be fit to the empirical expression (Datta et al., 1998)

$$\tau_p(n\sec) = 10^{\beta-\gamma\log N_D} \tag{4}$$

where N_D is the n+ InGaAs doping and the fit parameters are β=22.4, γ=1.2 for N_D > 8x10^{17} /cm^3. For smaller base doping than 8x10^{17} /cm^3, a constant lifetime of 10 ns was assumed. The empirical models for the concentration dependent minority carrier lifetime (Eq. (3) and Eq. (4)) were fit into the ATLAS Eq. (1) and Eq. (2) as shown in Fig. 3 (a) and Fig. 3 (b). Values for the fit are given in Table 2 (Menon et al. 2010).

The negative differential mobility model of Barnes et al. (1996) was used to account for the carrier drift velocity that peaks at some electric field before reducing as the electric field increases. The model is given by (Silvaco, 2004):

$$\mu(E) = \frac{\mu_0 + \frac{v_{sat}}{E}\left(\frac{E}{E_{crit}}\right)^{\gamma}}{1+\left(\frac{E}{E_{crit}}\right)^{\gamma}} \tag{5}$$

where v_{sat} is the carrier saturation velocity, E_{crit} is the critical electric field, E_0 and γ are constants and μ_0 is the low-field carrier mobility. The model parameters used for InGaAs are shown in Table 2 as well.

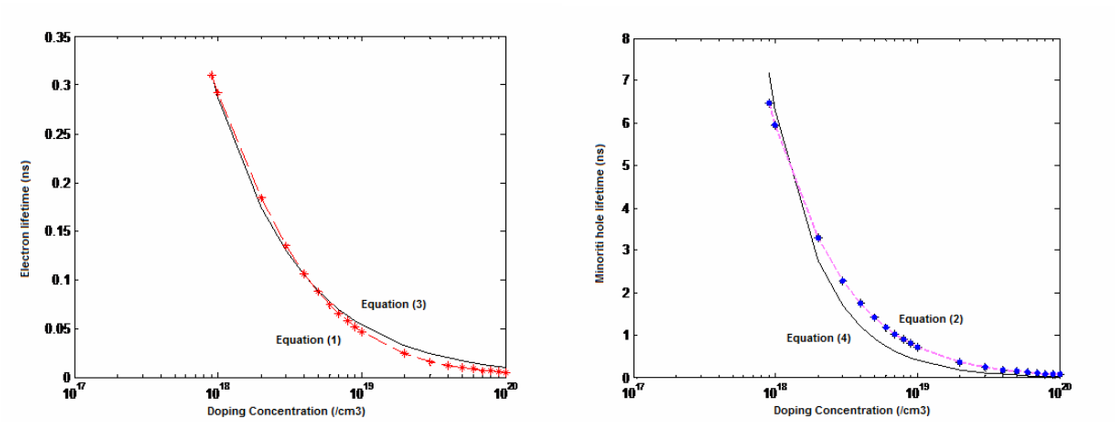

(a) (b)

Fig. 3. Fit of (a) concentration dependent minority electron lifetime in p+ InGaAs and (b) concentration dependent minority hole lifetime in n+ InGaAs (Source: Menon et al. 2010)

Parameters	Symbol	Units	Electrons	Holes
Concentration-dependent minority carrier lifetime model				
Lifetime	τ_0	Ns	0.6985	31.02
Total impurity conc.	N_{SRH}	$1/cm^3$	7.134×10^{17}	2.37×10^{17}
Parallel electric field-dependent mobility model				
Saturation velocity	v_{sat}	cm/sec	2.5×10^7	5×10^6
Fit parameter	Γ		4	1
Critical electric field	E_{crit}	V/cm	3000	4000

Table 2. Summary of concentration-dependent minority carrier lifetime and parallel electric field-dependent mobility model parameters (Source: Menon et al. 2010)

3.3 Low-field carrier mobility models

The electron and hole mobilities in $In_{0.53}Ga_{0.47}As$ (InGaAs) as a function of doping concentration and temperature are important parameters for device design and analysis. The default low field mobility parameters for InGaAs carriers in commercial device simulation packages are given by linear interpolations from the binary compounds of GaAs and InP (Silvaco, 2004) which do not describe the dependency of carrier mobility on doping concentration or temperature. Therefore, in this chapter, we attempt to provide the fitted parameters of a concentration- and temperature-dependent carrier mobility model to accurately characterize an InGaAs ILPP (Menon et al., 2008a).

The dependence of electron and hole low-field mobilities on doping and temperature (Caughey & Thomas, 1967) for electrons and holes is given by Eq. (6) and Eq. (7) respectively.

$$\mu_n = mu1n.caug.(\frac{T_L}{300K})^{alphan.caug} + \frac{mu2n.caug.(\frac{T_L}{300K})^{betan.caug} - mu1n.caug.(\frac{T_L}{300K})^{alphan.caug}}{1+(\frac{T_L}{300K})^{gamman.caug}.(\frac{N}{ncritn.caug})^{deltan.caug}} \quad (6)$$

$$\mu_p = mu1p.caug.(\frac{T_L}{300K})^{alphap.caug} + \frac{mu2p.caug.(\frac{T_L}{300K})^{betap.caug} - mu1p.caug.(\frac{T_L}{300K})^{alphap.caug}}{1+(\frac{T_L}{300K})^{gammap.caug}.(\frac{N}{ncritp.caug})^{deltap.caug}} \quad (7)$$

where N is the total impurity doping (cm^{-3}) and T_L is the lattice temperature (K). *mu1n.caug*, *mu1p.caug*, *mu2n.caug*, and *mu2p.caug* are the minimum and maximum mobilities of electrons and holes respectively (cm^2/V-s). The fitting parameters are *alphan.caug*, *alphap.caug*, *betan.caug*, *betap.caug*, *gamman.caug*, *gammap.caug*, *deltan.caug* and *deltap.caug* whereas *ncritn.caug* and *ncritp.caug* are the critical doping densities (cm^{-3}) for electrons and holes, respectively above which ionized impurity scattering becomes dominant (Menon et al., 2008a).

The mobility data has been fit to Eqs. (6) and (7) by Datta et al. (1998) for InGaAs at T_L=300K where *mu1n.caug*=3372, *mu1p.caug*=75, *mu2n.caug*=11599, *mu2p.caug*=331, *ncritn.caug*=8.9×10^{16}, *ncritp.caug*=1×10^{18}, *deltan.caug*=0.76 and *deltap.caug*=1.37. In this work

we have obtained the remaining fitting parameters of Eqs. (6) and (7) using curve-fitting methodology where we obtained *alphan.caug*=0.437, *alphap.caug*=0.9222, *betan.caug*=1.818, *betap.caug*=1.058, *gamman.caug*=2.526 and *gammap.caug*=7.659.

A comparison between these fitted results versus the calculated carrier mobility from (Sotoodeh et al., 2000; Arora et al., 1992; Chin et al., 1995) as well as some experimental Hall data (Lee & Forrest, 1991; Ohtsuka et al., 1988; Pearsall, 1981) is shown in Fig. 4(a) till Fig. 4 (c) for T=77K, 100K and 200K. Fig. 4(d) shows the electron mobility as a function of temperature in InGaAs where calculated electron mobility from this work is compared to the experimental Hall data from Takeda et al. (1981). A very good agreement is obtained for temperatures >150K (Menon et al., 2008a).

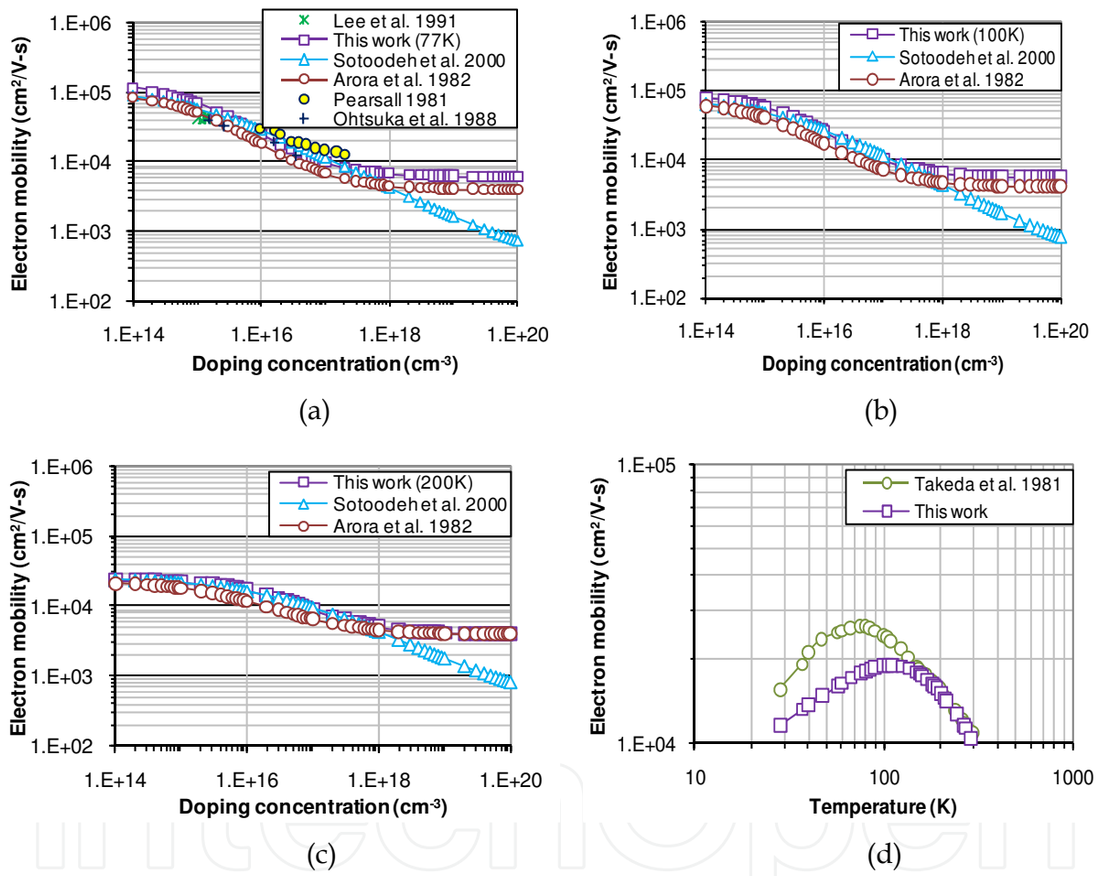

Fig. 4. Electron mobility in $In_{0.53}Ga_{0.47}As$ as a function of (a) doping at T_L=77K, (b) T_L=100K, (c) T_L=200K and (d) temperature at N=1.5e^{16}cm^{-3} (Source: Menon et al., 2008a)

The hole mobilities for InP-based material are similar to those seen for GaAs and AlGaAs (Datta et al., 1998). Fig. 5 (a) till Fig. 5 (c) show the fitted results versus calculated hole mobility for T=77K, 100K and 200K. Fig. 5(d) shows the hole mobility as a function of temperature in InGaAs. Good agreement is obtained for temperatures ≥200K.

Carrier mobility decreases sharply when doping density is increased for low doping densities (less than 1e18 cm^{-3}). For high doping densities, the mobility tends to decrease more slowly and shows a saturated trend. Similarly, for low operating temperatures (<100K), the carrier mobility tends to increase with increment in temperature. However,

above 100K, the mobility shows a downward bowing trend as temperature is increased. Therefore, it has been proven that the fitted parameters are reliable and match available experimental or theoretical data. These carrier mobility equations were used in the development of an ILPP based on InGaAs absorption layer.

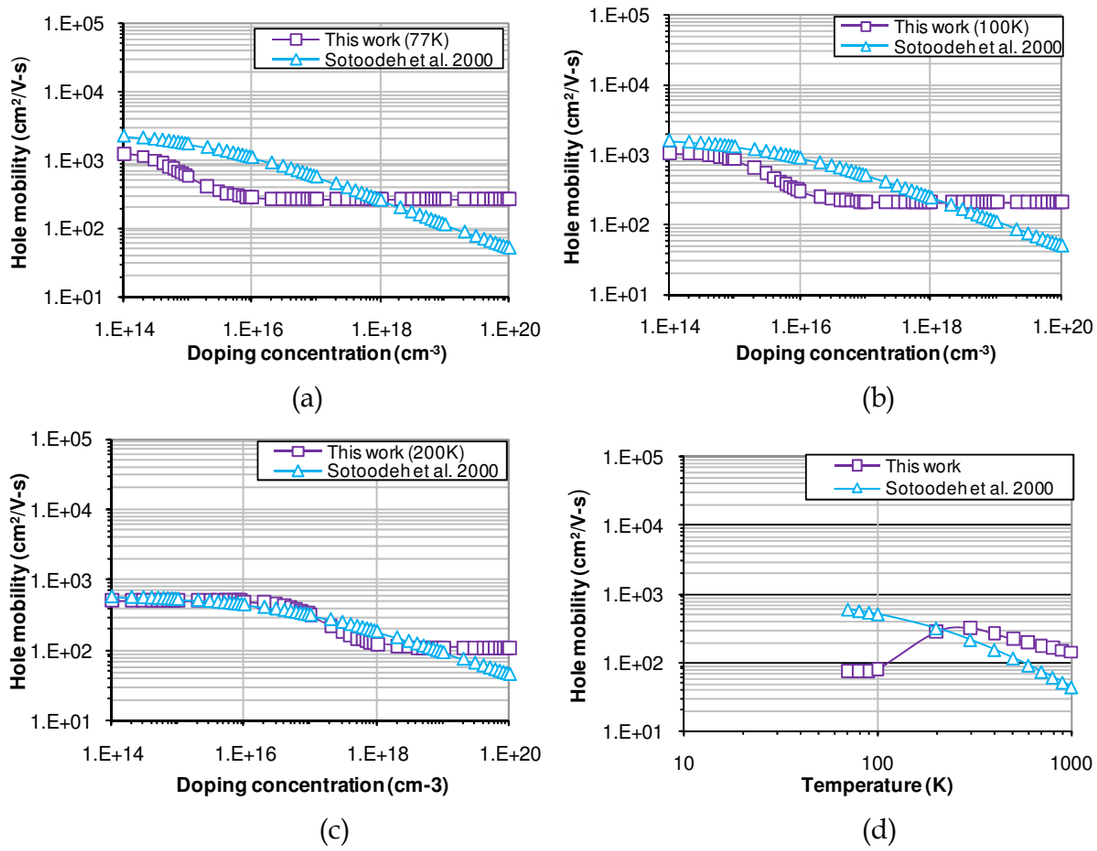

Fig. 5. Hole mobility in $In_{0.53}Ga_{0.47}As$ as a function of (a) doping at T_L=77K, (b) T_L=100K, (c) T_L=200K and (d) temperature at N=1e^{17}cm^{-3} (Source: Menon et al., 2008a)

4. Numerical modeling

4.1 Device material selection

InGaAs is specified as the absorbing material in ATLAS by setting the mol fraction of quaternary material $In_{1-x}Ga_xAs_yP_{1-y}$ where x=0.43 and y=1 to form $In_{0.53}Ga_{0.47}As$. It is used as the absorbing layer with a thickness of 3 μm and at this depth, 83% of the optical power will be absorbed by the device based on the InGaAs absorption coefficient, α=6070 /cm at λ=1.55 μm. The absorbing layer is also given an n-type background doping of 1e11 cm^{-3} with a uniform doping profile.

The p+ wells in the ILPP device will be formed using zinc SOD hence the junction parameters were obtained from available experimental data. Kamanin et al. (1996) formed a p+ junction in InGaAs using thin film zinc-based polymer diffusion at a temperature of 500˚C for 30 minutes to obtain junction depth of 0.8 μm and dopant surface concentration of ~8x10^{18} cm^{-3}. Similarly, in the ILPP model, the junction depth of the p+ wells was selected to

be 0.8 µm with a surface doping level of $4x10^{18}$ cm^{-3}. The n+ wells in InGaAs is proposed to be formed using selenium-doped SOD. Penna et al. (1985) performed ion implantation of Se into InGaAs to form a junction of ~0.4 µm deep. Alternatively, selenium-doped SOD have been used on GaAs to obtain junctions with a depth of 1.3 µm and surface concentration of $6x10^{18}$ cm^{-3} (Filmtronics, 2006). In this ILPP model, the junction depth of the selenium-doped n+ wells were set to be 0.8 µm with a surface concentration of $1x10^{19}$ cm^{-3} to produce a uniform electric field between the alternating junctions.
Spin-on glass (SOG) will be used as the passivation layer for InGaAs. It will serve to protect the junction surfaces as well as for planarizing the device. In this model, a 0.1-µm thick SiO_2 was used to reflect the presence of SOG on top of the SOD-doped InGaAs absorbing layer. Finally, the alternating interdigitated fingers were modelled as gold-based.

4.2 Design of device structure

The electrode finger width/ spacing and length are 1 µm and 50 µm respectively. The device's active area is 41 x 5 x 50 $µm^3$ with a total of 10 pairs of interdigitated electrodes. The junction depth for both the p+/n+ wells are 0.8 µm respectively and lateral diffusion per well is 0.3 µm. The compensation ratio θ (N_A/N_D) is set at 0.1 where donor concentration, $N_D=1e^{19}$ cm^{-3}. Fig. 6 shows the potential of the InGaAs ILPP three-dimensional model upon illumination of an optical beam with spectral width of 41 µm, optical spot power of 10 W/cm2 and wavelength, λ=1.55 µm.

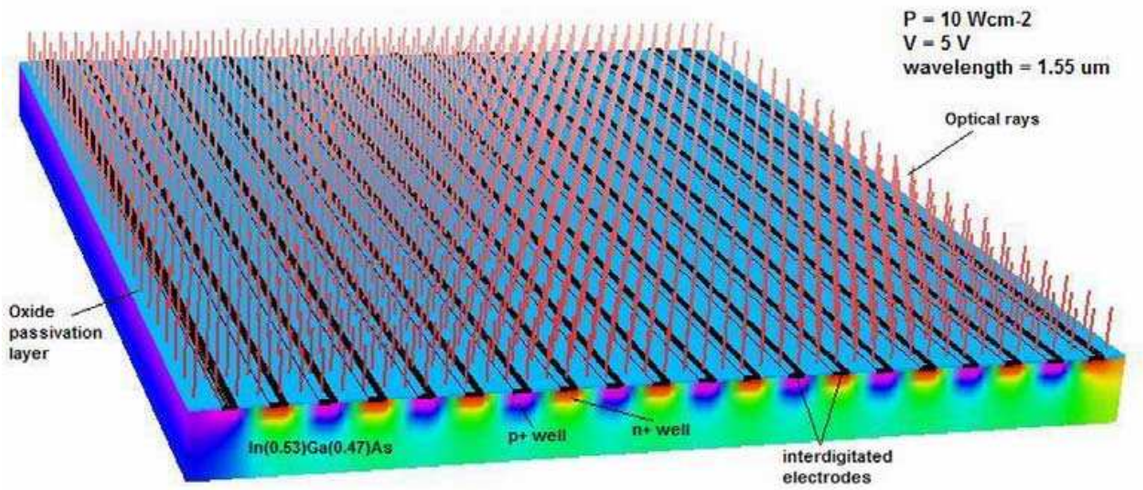

Fig. 6. Potential within the InGaAs ILPP 3D model upon illumination of an optical beam

4.3 Characterization equations

The ILPP dark current, I_D is given by:

$$I_D = I_{SAT}(e^{\frac{qV_A}{k_BT}} - 1) \tag{8}$$

where I_{SAT} is the reverse saturation current, q is the electron charge, V_A is the applied bias voltage, k_B is the Boltzmann constant and T is the absolute temperature in Kelvin. Illuminating the photodiode with optical radiation, shifts the I-V curve by the amount of photocurrent (I_P). Thus, the total current I_T is given by $I_T = I_D + I_P$.

The ILPP responsivity, R is calculated using:

$$R = \frac{I_T}{I_S}\left(\frac{\lambda}{1.24}\right) \tag{9}$$

where I_S is the source photocurrent and λ is the optical wavelength.
The simulator calculates the real (I_R) and imaginary (I_I) component current values for every equivalent AC frequency value. Hence, the -3dB frequency (f_{-3dB}) is calculated using the following equation:

$$f_{-3dB} = 20 * \log\left(\frac{I_R}{I_{R_0}}\right) \tag{10}$$

where I_{R0} is the real component current at low AC frequencies which is normally a constant value. Finally, the ILPP signal-to-noise ratio (SNR) is calculated using the following equation

$$SNR = \frac{\left\langle i_p^2 \right\rangle}{2q(I_p + I_D)B + 4k_BTB / R_L} \tag{11}$$

where I_P is the average photocurrent, B is the bandwidth and R_L is the load resistance set to be as 50 Ω (Menon et al. 2010).

4.4 Device characterization results

A cross section of the 3D device is shown in Fig. 7 (a) portraying the net doping within the device. Dark current value at 5 V was measured to be 21 nA and is much higher than that achieved by conventional InGaAs VPDs (in pA values) (Huang et al., 2007) due to the absence of a capping layer such as InP to reduce the surface leakage current. However, the modelled device's dark current is comparable to conventional ILPP that have been fabricated before as portrayed in Fig. 7 (b). The ideality factor, n was measured to be ~1 and the series as well as dynamic resistances were measured to be 43 Ω and ~238 MΩ respectively. Breakdown voltage was >40 V.
The capacitance values recorded at a bias voltage of 5V was 2.87 nF and this value is much higher than the capacitance values achieved by conventional ILPP devices due to the smaller intrinsic region width (1 µm in this design versus 3 µm in (Yasuoka et al., 1991)) and longer electrode fingers in the current design (50 µm in this design versus 20 µm and 47 µm in (Tiwari et al., 1992) and (Lee et al. 1989)). The C-V results are shown in Fig. 8(a).
Dark and photo-IV curves for the optical beam at λ=1.55 µm and P=dark (0), 1, 5, 10, 50, 100 and 200 Wcm^{-2} is shown in Fig. 8 (b). At operating voltage of 5V, the photocurrent increased from 0.011 mA (P=1 Wcm^{-2}) to 2.28 mA (P=200 Wcm^{-2}).
Fig. 9(a) is the responsivity curve of the modelled device at P=10 Wcm-2, V=5V and the wavelength is swept up from 0.75 µm until 1.75 µm. In optical communication networks, data signals are usually transmitted at λ=1.31 µm whereas video signals are transmitted at λ=1.55 µm. At both these wavelengths, the responsivity was measured to be 0.55 A/W and 0.56 A/W respectively which is equivalent to an external quantum efficiency of 44 %. These values are comparable to the experimentally developed InGaAs ILPP devices but are much smaller than VPDs due to the electrode shadowing effect in ILPP designs. Fig. 9(b) shows

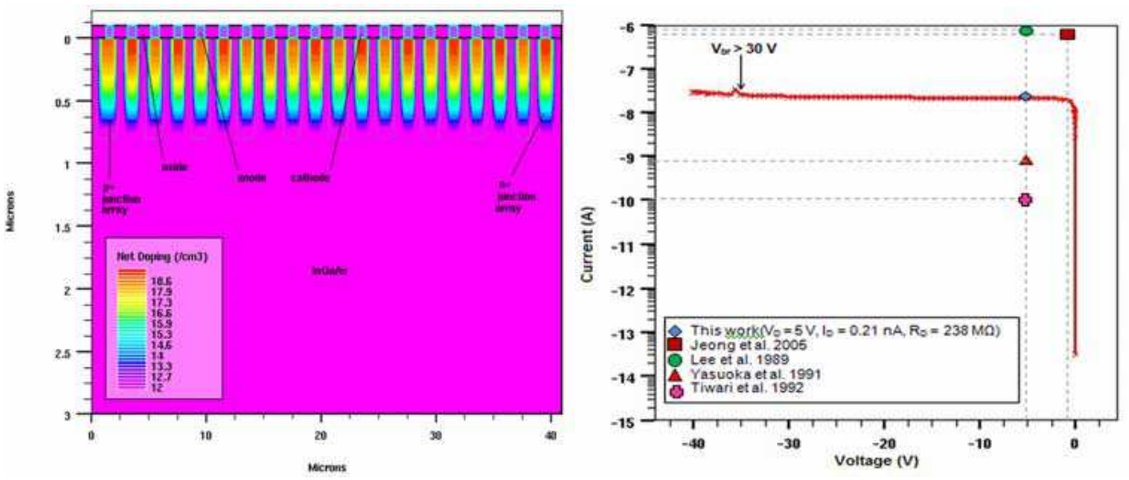

(a) (b)

Fig. 7. The ILPP's (a) cross section of the 3D device portraying the net doping within the device and (b) dark current trend (Source: Menon et al. 2010)

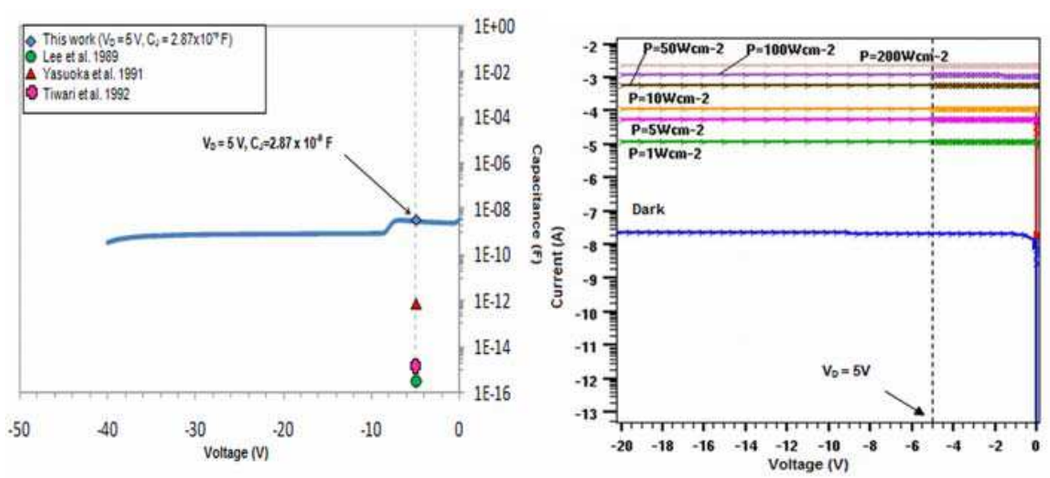

(a) (b)

Fig. 8. The ILPP's (a) C-V trend and (b) dark and photo-IV curves for the optical beam at λ=1.55 μm and P=dark (0), 1, 5, 10, 50, 100 and 200 Wcm^{-2} (Source: Menon et al. 2010)

the -3dB frequency of 8.93 GHz achieved by the model and it is 16% higher than conventional ILPP prototypes (Yasuoka et al., 1991; Tiwari et al., 1992; Lee et al. 1989; Jeong et al., 2005) mainly due to the smaller intrinsic region width utilized in this design.

The dark current noise is 0.06 fA/√Hz, quantum noise is 0.33 nA/√Hz and Johnson noise is 2.96 pA/√Hz with load resistance of 50 Ω where the Johnson noise is the highest noise contributor. The device SNR was calculated to be ~36 dB and dynamic range ranges from -16 dBm until 17.9 dBm (Menon et al. 2010).

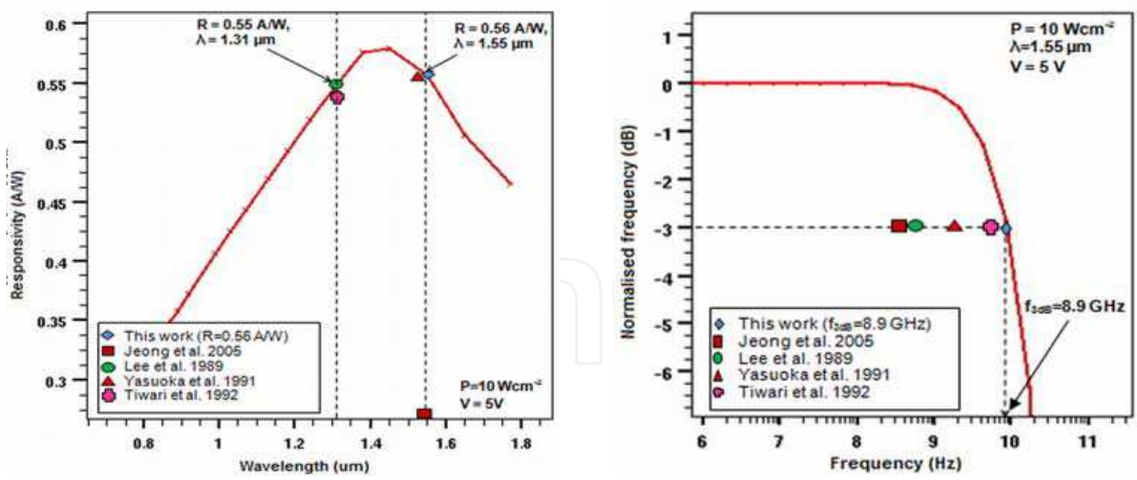

(a) (b)

Fig. 9. The ILPP's (a) responsivity curve of the modeled device at P=10 Wcm-2, V=5V and (b) the -3dB frequency (Source: Menon et al. 2010)

5. Statistical modeling

5.1 Fractional Factorial Design

Fractional factorial design (FFD) was used to identify the factors that affect the device responsivity significantly. Next, the significant factors were used to develop a general linear model to predict the responsivity of different ILPP models. In this research, seven factors i.e. InGaAs absorbing layer thickness (T), finger width (FW), finger spacing (FS), junction depth (JD), finger length (FL), bias voltage (V) and optical beam power (P) were investigated, each of which were tested at two levels. A one-quarter fractional factorial design (resolution IV) comprising of 32 runs (Montgomery, 2001) was carried out to obtain information on the effects of the investigated factors. Fig. 10 displays the ILPP model where the chosen factors are highlighted. Table 3 lists the factors and their respective values which were used in the DOE. A well-known statistical software, Minitab was used to obtain the statistical results (Menon et al. 2008b).

The normal probability plots and the pareto chart for the device responsivity are shown in Fig. 11 (a) and Fig. 11 (b). The significant factors which include interactive factors are highlighted in red in the normal probability plots. Significant or active effects are larger and further away from the fitted line than inactive effects which tend to be smaller and centered around zero, the mean of all the effects. The pareto charts display the absolute value of the effects.

In the normal probability plot for the device responsivity, the most significant factor that affects this response is the InGaAs thickness (A), followed by the finger width (B), finger spacing (C) and the interaction factor between InGaAs thickness and finger width (A*B). These significant factors prove that when the absorbing layer thickness is increased, the absorbed optical power, $P(x)$ at a depth of x increases according to the equation $P(x)=P_0(1-e^{1-a(x)})$where P_0 is the incident optical power and a is the absorbing coefficient. Decrement in the electrode finger width (FW) and increment in the electrode finger spacing (FS) increases the total illumination area from the top of the device hence increasing the total generated photocurrent within the device and subsequently increases the device responsivity.

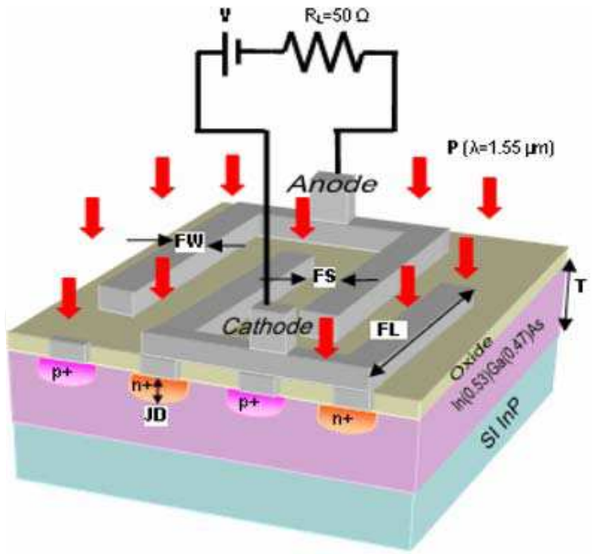

Fig. 10. Schematic diagram of the ILPP model. The chosen factors are highlighted in the diagram.

Variable (Code)	Factor name	-1 Level (Low)	+1 Level (High)
A(T)	InGaAs thickness (μm)	1	3
B(FW)	Finger width (μm)	1	3
C(FS)	Finger spacing (μm)	1	3
D(JD)	Junction depth (μm)	0.4	0.8
E(V)	Voltage (V)	2	5
F(P)	Beam power (Wcm^{-2})	1	10
G(FL)	Finger length (μm)	20	50

Table 3. Fractional factorial design factors and values.

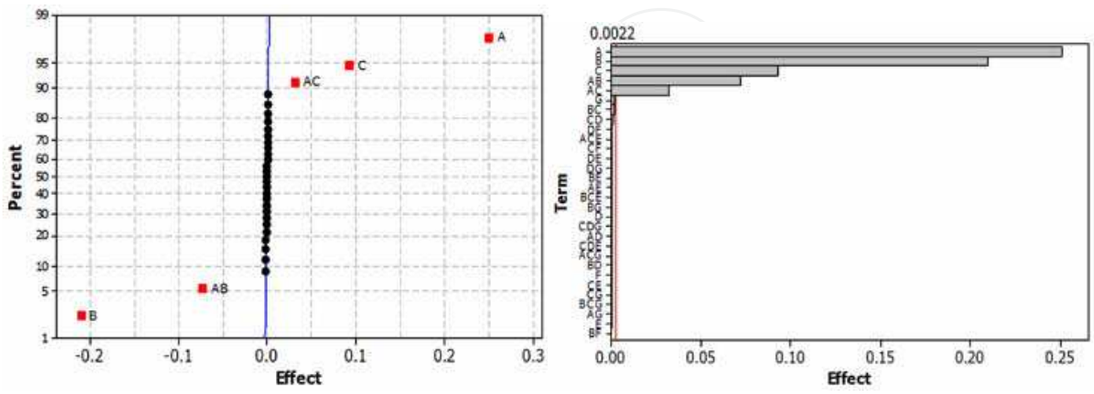

(a) (b)

Fig. 11. (a): Normal probability plot for the responsivity. The factors highlighted in red are significant and (b) Pareto chart for the responsivity displaying absolute values of the factor effects in descending order.

Next, the significant factors for the device responsivity was used to develop a reduced model at a confidence level of 95%. This was done by screening out the insignificant effects from the full model and evaluating the fit of the new reduced model using analysis of variance (ANOVA). The main effects as well as significant two-way interaction effects which are significant gives a *p*-value. If $p<0.05$, then the effect or term is significant whereas if $p>0.05$, then the terms are insignificant and hence can be excluded from the reduced model. From Fig. 16 and Fig. 17, the new reduced model will now comprise of the main effects (A, B and C) as well as two-way and three-way interactive factors which include these main effects. Table 4 lists the analysis of variance for the device responsivity using the factorial fit from the reduced model (Menon et al., 2009).

Term	**Effect**	**Coefficient**	***p*-value**
Constant		0.3564	0.000
T	0.2506	0.1253	0.000
FW	-0.2095	-0.1047	0.000
FS	0.0930	0.0465	0.000
T*FW	-0.0722	-0.0361	0.000
T*FS	0.0324	0.0162	0.000
FW*FS	-0.0017	-0.0008	0.034
T*FW*FS	-0.0009	-0.0005	0.221

Table 4. Analysis of variance for responsivity (S=0.002, R^2=99.9%, R^2(adj)=99.9%).

All the terms have a *p*-value of <0.05 except the last term (T*FW*FS) where the *p*-value is 0.221 deeming it insignificant. The *S*, R^2 and adjusted R^2 are measures of how well the model fits the data where *S* represents how far the standard distance data values fall from the regression line, R^2 describes the amount of variation in the observed response values and adjusted R^2 is a modified R^2 that has been adjusted for the number of terms in the model. For a given fit, the lower the value of *S* and the higher the values of R^2 and adjusted R^2, the better the equation predicts the response. In this model, values of *S*, R^2 and adjusted R^2 are 0.002 and 99.9% respectively proving that a robust model for predicting the InGaAs ILPP responsivity has been established. Next, the coefficients of each significant term is used to construct a regression or analytic equation representing the relationship between the device responsivity and the design factors. The regression equation which defines the responsivity of the InGaAs ILPP is as follows (Menon et al., 2009):

$$\begin{aligned} y_{(resp)} &= 0.3564 + 0.1253(T)_c - 0.1047(FW)_c \\ &+0.0465(FS)_c - 0.0361(T)_c(FW)_c \\ &+0.0162(T)_c(FS)_c - 0.0008(FW)_c(FW)_c \end{aligned} \tag{12}$$

where X_c is the factor value in coded units and it is related to the actual factor value X_a by

$$X_a = \frac{X_c - \left[\frac{(X_H + X_L)}{2}\right]}{\frac{(X_H - X_L)}{2}} \tag{13}$$

where X_L and X_H are the factor values at the low level and high level as given in Table 1. Eq. (13) can be rearranged to obtain the value of X_c:

$$X_c = \frac{(X_H + X_L)}{2} + \left\{\frac{(X_H - X_L)}{2}\right\} X_a \tag{14}$$

The coded values for all the factors which defines the device responsivity is calculated and is given as follows:

$$(T)_c = 2 + (T)_a \tag{15}$$

$$(FW)_c = 2 + (FW)_a \tag{16}$$

$$(FS)_c = 2 + (FS)_a \tag{17}$$

Eqs. (15) to (17) are replaced into Eq. (12) to obtain the general linear model which defines the responsivity of an InGaAs ILPP in uncoded units.

$$\begin{aligned} y_{(resp)} &= 0.143106 + 0.163188(T)_a - 0.0327433(FW)_a \\ &+0.0138567(FS)_a - 0.0351578(T)_a(FW)_a \\ &+0.0171634(T)_a(FS)_a - 0.000096781(FW)_a(FS)_a \end{aligned} \tag{18}$$

where T_a, FW_a, $FS_a \neq 0$.

5.2 Model verification

Eq. (18) was used to recalculate the responsivity of the numerical models used in the 32 runs of the fractional factorial DOE and the comparative results between the simulated and calculated values as well as the error ratios are displayed in Fig. 12. Good correlation is observed between the two values and the error ratios are less than 3% for all the 32 models. Table 5 lists the factor values of some InGaAs ILPP designs from previous experimental work. The responsivity of these devices were recalculated using Eq. (18) and error ratios between 16% to 27% were obtained between the actual and calculated responsivity values. The results are displayed in Fig. 13. The high error ratios could be attributed to the drift-diffusion model used in the simulation for ILPP devices whereas the actual devices were fabricated using different techniques where carrier transport model may vary. The simulated model also does not take into consideration fabrication

defects and reflects an ideal ILPP device. Eq. (18) is a new analytic equation which can be used to predict the responsivity of InGaAs ILPP as a function of the device design factors prior to fabrication.

No	T (μm)	FW (μm)	FS(μm)	Reference
1	1.7	1	3	Yasuoka et al., 1991
2	1.4	20	2	Tiwari et al., 1992
3	2	2	3	Lee et al., 1989

Table 5. Factor values from periodical literature

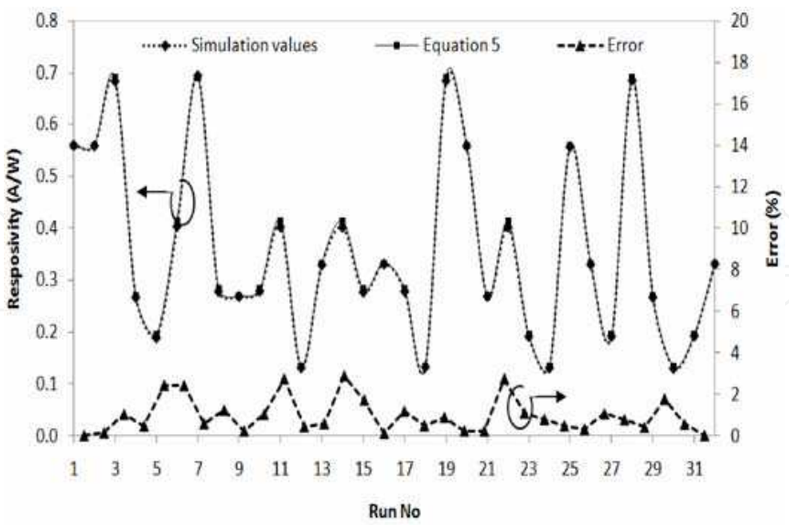

Fig. 12. Comparitive results between the simulated and calculated responsivity values from Eq. (18) as well as the error ratios.

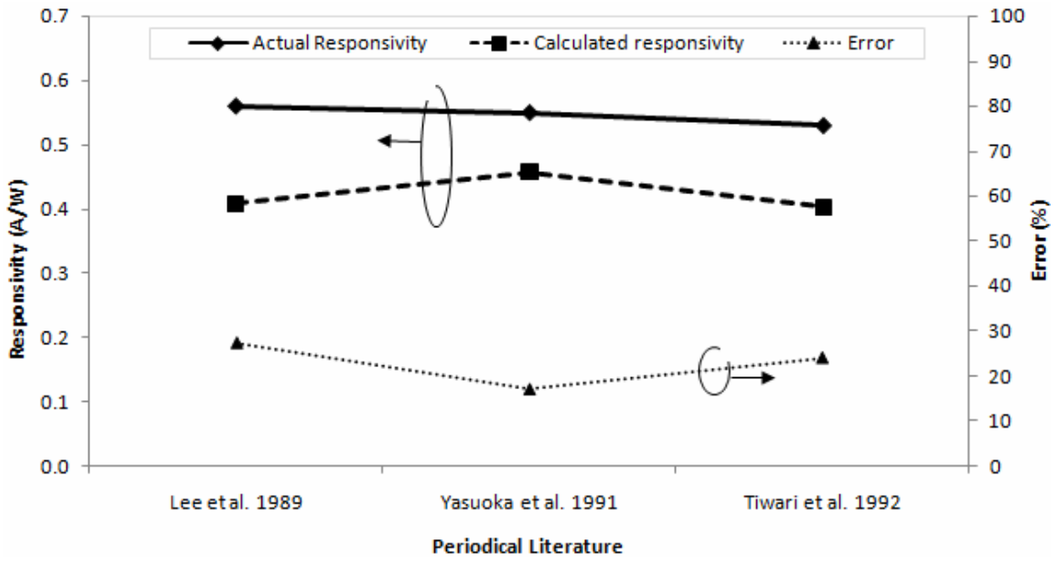

Fig. 3. Comparison between the actual responsivity versus calculated responsivity values using Eq. (18) for past experimentally developed devices.

5.3 Statistical optimization

A statistically optimized model for the InGaAs ILPP device was obtained by specifying the target range values that would like to be attained for each device characteristic. This is shown in Table 6. The optimized design factors that must be chosen in order to achieve the optimal target characteristic values as stipulated in Table 6 are given in Table 7. These optimized design factors can be used in the fabrication of InGaAs-based ILPP devices in the future.

Characteristics	Units	Low Target Value	High Target Value	Optimal Target Value
Responsivity	A/W	0.5	1	0.68
-3dB frequency	GHz	5	10	7.43
SNR	dB	10	50	12.11

Table 6. Target and optimal characteristic values obtained statistically

Variable (Code)	Factor name	-1 Level (Low)	+1 Level (High)	Optimal Target Value
A(T)	InGaAs thickness (μm)	1	3	3
B(FW)	Finger width (μm)	1	3	1
C(FS)	Finger spacing (μm)	1	3	3
D(JD)	Junction depth (μm)	0.4	0.8	0.8
E(V)	Voltage (V)	2	5	5
F(P)	Beam power (Wcm^{-2})	1	10	1.14
G(FL)	Finger length (μm)	20	50	20

Table 7. Target design factors for a statistically optimized InGaAs ILPP device

6. Conclusion

A novel interdigitated lateral p-i-n photodiode (ILPP) model utilizing $In_{0.53}Ga_{0.47}As$ as the absorbing layer was developed numerically and optimized statistically using fractional factorial methodology. Seven model factors were investigated and an analytical expression to predict the device responsivity was defined. Comparison between the simulated and calculated responsivity values yielded error ratios of less than 3%. Finally, a statistically optimized InGaAs ILPP model with -3dB frequency of 7.5 GHz, responsivity of 0.61 A/W and SNR of 20 dB was developed at an operating voltage of 5 V, wavelength of 1.55 μm and optical input power of 10 Wcm^{-2}. The modeled device provides a cheap and easy solution to cater for the increasing demand of FTTH-PON users

7. Acknowledgement

The authors would like to thank the Malaysian Ministry of Science, Technology and Innovation (MOSTI), the Malaysian Ministry of Higher Education (MOHE) and Universiti Kebangsaan Malaysia (UKM) for sponsoring this project under grants IRPA 03-02-02-0069-EA231 and UKM-OUP-NBT-27-119/2010

8. References

Adachi, S. (1992*). Physical properties of III-V Semiconductor Compounds: InP, InAs, GaAs, GaP, InGaAs and InGaAsP*, New York: Wiley Interscience.

Arora, N. D., Hauser, J.R. & Roulstan, R. J. (1982). Electron and hole mobilities in silicon as a function of concentration and temperature. *IEEE Transactions on Electron Devices* ED-29: 292.

Barnes, J. J., Lomax, R. J. & Haddad, G. I. (1996). Finite element simulation GaAs MESFET with lateral doping profiles and submicron gates. *IEEE Transactions on Electron Devices* ED-23: 1042-1048.

Caughey, D. M. & Thomas, R. E. (1967). Carrier mobilities in silicon empirically related to doping and field. *Proceedings of the IEEE*, 2192-2193.

Chin, W. L., Osotchan, T. & Tansley, T. L. (1995). Electron mobility in In(0.53)Ga(0.47)As as a function of concentration and temperature. *Microelectronics Journal* 26: 653-657.

Conklin, T., Naugle, S., Shi, S., Roenker, K. P., Frimel, S. M. Kumar, T & Cahay, M. M. (1996). Inclusion of tunneling and ballistic transport effects in an analytical approach to modeling of NPN InP based heterojunction bipolar transistors. *Superlattice Microstructures* 18: 1-12.

Cvetkovic, M., Matavulj, P., Radunovic, J. & Marincic, A. (2000). An InGaAs P-I-N photodiode model: Description and implementations in the analysis of the 1.55 μm lightwave system. *Journal of Optical Communications* 31(3): 35-39.

Datta, S., Shi, S., Roenker, K. P., Cahay, M. M. & Stanchina, W.E. (1998). Simulation and design of InAlAs/InGaAs pnp heterojunction bipolar transistors. *IEEE Transactions on Electron Devices*, 45(8): 1634-1643.

Dentan, M & Cremoux, B. D. (1990). Numerical simulation of the nonlinear response of a p-i-n photodiode under high illumination. *Journal of Lightwave Technology* 8: 1137-1144.

Diadiuk, V. & Groves, S. H. (1985). Lateral photodetectors on semi-insulating InGaAs and InP. *Applied Physics Letters* 46(2): 157-158.

Dildey, F., Treichler, R., Amann, M.-C., Schier, M. & Ebbinghaus, G. (1989). Replacement of magnesium in InGaAs/InP heterostructures during zinc diffusion. *Applied Physics Letters* 55(9): 876

Ehsan, A. A., Shaari, S. (2001). *Fabrikasi dan pencirian diodfoto planar P-I-N silikon untuk OEIC*. Technical Report No MTF 004. Universiti Kebangsaan Malaysia.

Feng, S. & Lu, C. (2004). Influence of InP cap layer on photo-responsivity of InP/InGaAs PIN detector. *Proceedings of the 7th International Conference on Solid-State and Integrated Circuits Technology*, 2332-2334.

Filmtronics, Incorporated. (2006a). *Experimental Selenium Film Se-965*. Datasheet. USA.

Filmtronics, Incorporated. (2006b). *Experimental Zinc Zn-980*. Datasheet. USA.

Gangopadhyay, U., Park, S., Kim, K., Park, J., Kim, D. & Yi, J. (2003). Large area monocrystalline silicon solar cell using SOD. *Proceedings of 3rd World Conference on Photovoltaic Energy Conversion*, 1431-1434.

Giziewicz, W., Prasad, S. & Fonstad, C. G. Jr. (2004). Lateral p-i-n photodetectors fabricated in a standard commercial GaAs VLSI process. *Proceedings of IEEE on Sensors*, 284-287

Goodrich Corporation. (2006). What is InGaAs?. Application Note 4110-0039: 1-3. http://www.sensorsinc.com/GaAs.html

Ho, C.-L., Wu, M.-C., Ho, W.-J. & Liaw, J.-W. (2000). Comparison between planar InP/InGaAs/InP pin photodiodes with symmetrical and asymmetrical doping profiles. *IEEE Proceedings on Optoelectronics* 147(2): 109-113.

Huang, Z. (2003). *Multi gigahertz InGaAs/InP inverted MSM photodetectors for photoreceiver and waveguide applications*. Ph.D Thesis. Georgia Institute of Technology, Atlanta.

Jacob, B., Witzigmann, B., Klemenc, M. & Petit, C. (2005). A TCAD methodology for high-speed photodetectors. *Solid -State Electronics* 49: 1002-1008.

Jeong, T.W.; Iiyama, K.; Takamiya, S. (2005). Two terminal InP/InGaAs heterojunction phototransistor with lateral photodiode as sensing section. *International Conference on Indium Phosphide and Related Materials*, 250-253.

Kamanin, A. V., Mokina, I. A., Shmidt, N. M., Busygina, L. A., & Yurre, T. A. (1996). Polymer diffusants in III-V semiconductor compounds technology. *Proceedings of the Eighth International Conference on Indium Phosphide and Related Materials IPRM '96*, 334-337

Kim, K. S. (2003). On the evolution of PON-based FTTH systems. *Information Sciences* 149: 21-30.

Koester, S. J., Schaub, J. D., Dehlinger, G & Chu, J. O. (2006). Germanium-on-SOI infrared detectors for integrated photonic applications. *IEEE Journal of Selected Topics in Quantum Electronics* 12(6): 1489-1502.

Konno, K., Matsushima, O., Navarro, D. & Miura-Mattausch, M. (2004). High frequency response of p-i-n photodiodes analyzed by an analytical model in Fourier space. *Applied Physics Letters* 96(7): 3839-3844.

Lange, M. J., Dixon, & Olfsen, G. H. (2000). p-n junction formation in 3- and 4-inch indium gallium arsenide epitaxial wafers using a doped glass diffusion source. *Conference on Lasers and Electro-Optics (CLEO 2000)*, 351-352.

Lauterbach, C. (1995). Zinc diffusion in InP from spin-on films of various zinc concentrations. *Semiconductor Science and Technology* 10: 500-503.

Lee, B., Yoon, H., Hyun, K. S., Kwon, Y. H. & Yun, I. (2004). Investigation of manufacturing variations of planar InP/InGaAs avalanche photodiodes for optical receivers. *Microelectronics Journal* 35(8): 635-640.

Lee, C. D & Forrest, S. R. (1991). $In_{0.53}Ga_{0.47}As$/InP heterojunction with low interface defect densities. *Journal of Applied Physics* 69: 342.

Lee, C.-H. & Choi, K.-M. (2007). Fiber to the home. *IEEE Proceedings*. 937-938

Lee, W. S., Kitching, S. A. & Bland, S. W. (1989). Monolithic integration of fully ion-implanted lateral GaInAs pin detector/InP JFET amplifier for 1.3-1.55 μm optical receivers. *Electronics Letters* 25(8): 522-523.

Li, R., Schaub, J. D., Csutak, S. M., & Campbell, J. C. (2000). A high-speed monolithic silicon photoreceiver fabricated on SOI; *IEEE Photon. Technol. Lett.* 12:1046-1048.

Loo, E. C. H. 2007. *Pembangunan diodfoto planar silicon dan InGaAs dengan elektrod* H_N *dan* H_P. Ph.D. Thesis. Universiti Kebangsaan Malaysia.

Menon, P. S. (2005). *Pembangunan diodfoto planar p-i-n silikon (Development of silicon-based p-i-n photodiode)*. MSc Thesis. Universiti Kebangsaan Malaysia.

Menon, P. S., Kandiah, K., Ehsan, A. A. & Shaari, S. (2009). The development of a new responsivity prediction model for In(0.53)Ga(0.47)As interdigitated lateral PIN photodiode. *Journal of Optical Communications*, 30, 2009: 2-6.

Menon, P. S., Kandiah, K. & Shaari, S. (2008a). Concentration and temperature-dependent low-field mobility model for In0.53Ga0.47As interdigitated lateral PIN PD. *IEICE Electronics Express* 5(9): 303-309.

Menon, P. S., Kandiah, K. & Shaari, S. (2008b). SNR prediction model of an In(0.53)Ga(0.47)As interdigitated lateral p-i-n photodiode. *Proceedings of the 2008 IEEE International Conference on Semiconductor Electronics*, ICSE2008 (Johor Bahru), 292-296.

Menon, P. S., Kandiah, K., Ehsan, A. A. & Shaari, S. (2010). Concentration-dependent minority carrier lifetime in an In(0.53)Ga(0.47)As interdigitated lateral PIN

photodiode based on spin-on chemical fabrication methodology. *International Journal of Numerical Modelling: Electronic Networks, Devices and Fields*. DOI: 10.1002/jnm.792

Menon, P. S. (2008). *Pembangunan diodfoto planar p-i-n In(0.53)Ga(0.47)As dengan elektrod berselang-seli (Development of an In(0.53)Ga(0.47)As interdigitated lateral p-i-n photodiode)*. Ph.D Thesis. Universiti Kebangsaan Malaysia.

Montgomery, D.C. (2005). *Design and analysis of experiment*. 6th Edition. New York: John Wiley.

Murray, S. L., Newman, F. D., Wilt, D. M., Wanlass, M. W., Ahrenkiel, P., Messham, R. & Siergiej, R. R. (2003). MOCVD growth of lattice-matched and mismatched InGaAs materials for thermophotovoltaic energy conversion. *Semiconductor Science and Technology* 18: 202-208.

Oh, J., Im, K., Ahn, C-G., Yang, J-H., Cho, W-J., Lee, S. & Park, K. (2004). Ultra shallow and abrupt n+–p junction formations on silicon-on-insulator by solid phase diffusion of arsenic from spin-on-dopant for sub 50 nm Si metal-oxide-semiconductor devices. *Materials Science and Engineering B* 110(2): 185-189.

Ohtsuka, K., Ohishi, T., Abe, Y., Sugimoto, H., Matsui, T. & Ogata, H. (1988). High purity $In_{0.53}Ga_{0.47}As$ layer grown by liquid phase epitaxy. *Journal of Crystal Growth* 89: 391.

Parker, D.G. (1988). The theory, fabrication and assessment of ultra high-speed photodiodes. *GEC Journal of Research* 6(2): 106-117.

Pearsall, T. P. (1981). Alloy scattering effects and calculated mobility in n-type $Ga_{0.47}In_{0.53}As$. *Electronics Letters* 17: 169.

Penna, T., Tell, B., Liao, A. S. H., Bridges, T. J. & Burkhardt, G. (1985). Ion implantation of Si and Se donors in $In_{0.53}Ga_{0.47}As$. *Journal of Applied Physics* 57(2): 351-354.

Posthuma, N. E., van der Heide, J., Flamand, G. & Poortmans, J. (2007). Emitter formation and contact realization by diffusion for germanium photovoltaic devices. *IEEE Transactions on Electron Devices* 54(5): 1210-1215.

Sabella, R. & Merli, S. (1993). Analysis of InGaAs P-I-N photodiode frequency response. *IEEE Journal of Quantum Electronics* 29:906-916.

Saleh, B. E. A. & Teich, M.C. (1991). *Fundamentals of photonics.* USA: John Wiley & Sons Incorporated.

Schow, C.L., Li, R., Schaub, J.D. & Campbell, J.C. (1999). Design and implementation of high-speed planar Si photodiodes fabricated on SOI substrates. *IEEE Journal of Selected Topics in Quantum Electronics* 35(10): 1478-1482.

Sipahi, L.B. & Sanders, T. J. (2002). Modeling, simulation and comparative analysis of RF bipolar and MOS low noise amplifiers for determining their performance dependence on silicon. *Proceedings of the fifth international conference on modeling and simulation of Microsystems MSM2002*, 155-158.

Srivastava, S. & Roenker, K.P. (2003). Numerical modeling study of the InP/InGaAs uni-travelling carrier photodiode. *Solid -State Electronics* 48: 461-470.

Sze, S.M. 2002. *Semiconductor Devices, Physics and Technology*. 2nd Edition. New York: John Wiley & Sons.

Tiwari, S., Burroughes, J., Milshtein, M. S., Tischler, M. A. & Wright, S. L. (1992). Lateral Ga(0.47)In(0.53)As and GaAs p-i-n photodetectors by self-aligned diffusion. *IEEE Photonics Technology Letters* 4(4): 396-398.

Tsang, W. T. (1985). Semiconductors and Semimetals. In *Lightwave Communications Technology*. New Jersey: Academic Press.

Silvaco International. (2004). *ATLAS User's Manual*. 10th Edition. USA: SILVACO International Incorporated.

Sotoodeh, M., Khalid, A. H. & Rezazadeh, A. A. (2000). Empirical low-field mobility model for III-V compounds applicable in device simulation codes. *Journal of Applied Physics* 87: 2890-2900.

Takeda, Y., Littlejohn, M. A. & Hauser, J. R. (1981). Electron Hall mobility calculation and alloy scattering in $In_{0.53}Ga_{0.47}As$. *Electronics Letters* 17: 377.

Tashima, M. M., Cook, L. W. & Stillman, G. E. (1981). Room temperature electron diffusion lengths in liquid phase epitaxial InGaAsP and InGaAs. *Applied Physics Letters* 39: 960-961.

Yasouka, N., Sanada, T., Hamaguchi, H., Makiuchi, M., Mikawa, T., Kuramata, A., Wada, O., Deri, R.J. (1991). High-speed monolithic coherent optical receiver integrated on InP substrate. *Electronics Letters* 27(22): 2020-2022.

Yuan, C-A., Han, C. N., Yew, M-C.,Chou, C-Y. & Chiang, K-N. (2005). Design, analysis and development of novel three-dimensional stacking WLCSP. *IEEE Transactions on Advanced Packaging* 28:387-396.

Zant, P. V. (2000). *Microchip fabrication*. USA: McGraw-Hill.

Zhao, X. (2006). *Carrier transport in high-speed photodetectors based on two-dimensional-gas*. Ph.D Thesis. Drexel University.

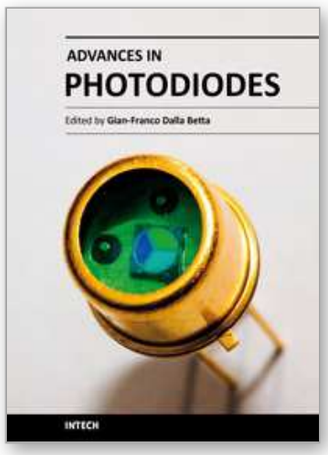

Advances in Photodiodes

Edited by Prof. Gian Franco Dalla Betta

ISBN 978-953-307-163-3
Hard cover, 466 pages
Publisher InTech
Published online 22, March, 2011
Published in print edition March, 2011

Photodiodes, the simplest but most versatile optoelectronic devices, are currently used in a variety of applications, including vision systems, optical interconnects, optical storage systems, photometry, particle physics, medical imaging, etc. Advances in Photodiodes addresses the state-of-the-art, latest developments and new trends in the field, covering theoretical aspects, design and simulation issues, processing techniques, experimental results, and applications. Written by internationally renowned experts, with contributions from universities, research institutes and industries, the book is a valuable reference tool for students, scientists, engineers, and researchers.

How to reference

In order to correctly reference this scholarly work, feel free to copy and paste the following:

P Susthitha Menon, Abang Annuar Ehsan and Sahbudin Shaari (2011). Modeling and Optimization of Three-Dimensional Interdigitated Lateral p-i-n Photodiodes Based on In0.53Ga0.47As Absorbers for Optical Communications, Advances in Photodiodes, Prof. Gian Franco Dalla Betta (Ed.), ISBN: 978-953-307-163-3, InTech, Available from: http://www.intechopen.com/books/advances-in-photodiodes/modeling-and-optimization-of-three-dimensional-interdigitated-lateral-p-i-n-photodiodes-based-on-in0

INTECH
open science | open minds

InTech Europe
University Campus STeP Ri
Slavka Krautzeka 83/A
51000 Rijeka, Croatia
Phone: +385 (51) 770 447
Fax: +385 (51) 686 166
www.intechopen.com

InTech China
Unit 405, Office Block, Hotel Equatorial Shanghai
No.65, Yan An Road (West), Shanghai, 200040, China
中国上海市延安西路65号上海国际贵都大饭店办公楼405单元
Phone: +86-21-62489820
Fax: +86-21-62489821

IntechOpen